Supporting information for: The rational design of allosteric inhibitors and activators using the population-shift model: *in vitro* validation and application to an artificial biosensor

Francesco Ricci, Alexis Vallée-Bélisle, Alessandro Porchetta and Kevin W. Plaxco

I-SUPPORTING METHODS

HPLC purified oligonucleotides internally modified with a FAM (5-carboxyfluorescein) and a BHQ-1 (black hole quencher 1) were purchased from Biosearch Technologies (Novato, CA). FAM and BHQ-1 were linked to these oligonucleotides via the C5-position of a thymine. Target and allosteric effector oligonucleotides were purchased from Sigma-Genosys. The sequences of the beacons and their allosteric effectors were as follows.

Inhibited molecular beacon (MB#1): 5'-CGG AAT TAA TCT CTT TG T**(FAM)**TTCCC *GAT CGG CGT TTT A* GGGAAT**(BHQ)** GGT TCA TCA TCA ACT AG-3'

Inhibitor: 5'-TGA TGA ACC CAC AAA GAG ATT-3'

Activated molecular beacon (MB#2): 5'-CGG AAT TAA TCT CTT TG CTCT**(FAM)**TTCCC *GAT CGG CGT TTT A* GGGAAT**(BHQ)**GAG GGT TCA TCA TCA ACT AG-3'

Activator: 5'-AGA GCA AAG AGA TT-3'

In the molecular beacon sequences above the underlined bases represent the stem portion, while the italic bases represent the recognition element (loop portion). Both molecular beacons recognize the same 13-base target (5'-TAAAACGCCGATC-3'). For mismatch discrimination experiments the following 1-base mismatch was tested (5'-TAAAGCGCCGATC-3') where the underlined base represents the mismatch.

All experiments were conducted in 50 mM sodium phosphate, 150 mM NaCl, pH 7.0 at 45°C. All fluorescence measurements were obtained using a Cary Eclipse Fluorimeter with excitation at 480 (± 5) nm and acquisition between 514 and 520 nm.

Allosteric inhibition: We employed molecular beacon MB#1 for our inhibition studies (see above for sequence). In the absence of target, inhibitor binding produces a small, but detectable decrease in signal (presumably because it moves the fluorophore slightly closer to the quencher) that we used to determine the inhibitor's binding curve and, in turn, K_i (Figure S1). Binding curves of probe/inhibitor reaction were obtained using a concentration of molecular beacon (MB#1) of 10 nM. Solutions with increasing concentration of inhibitor (plus 10 nM MB#1) were added to a 10 nM MB#1 solution and the fluorescence signal was recorded every 5 minutes until it reached equilibrium (Figure S3). Similarly, probe/target binding curves were obtained using 10 nM MB#1 in the presence of the relevant concentration of inhibitor. Solutions of increasing target concentration (plus 10 nM conc MB#1 and the same concentration of inhibitor initially used) were added to the molecular beacon solution and the fluorescence signal was recorded every 5 minutes until it reached equilibrium.

Binding curves were fitted to a single-site binding mechanism ([X] = target or inhibitor concentration; F_B= fluorescence in the presence of saturating concentration of target; $F_{[T]}$= fluorescence in the presence of different concentration of target; F_o = background fluorescence):

$$F_{[T]} = F_0 + \left(\frac{[\mathrm{X}](F_B - F_0)}{[\mathrm{X}] + K_d} \right) \qquad \text{Eq. S1}$$

To test the population-shift model it was necessary to measure the affinity of the inhibitor for the molecular beacon (K_i), a requirement that informed the design of our allosteric effectors. To this end we optimized the length of the inhibitor such that its K_i was within the range that we could measure experimentally; longer inhibitor sequences, which bind more tightly, produced K_i well below those we could measure given the 10 nM molecular beacon concentration we employed.

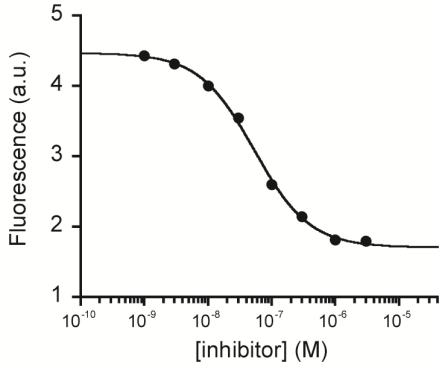

Figure S1. The addition of the allosteric inhibitor causes a small but detectable signal decrease (about 4% of the signal change seen at saturating target concentrations) that we used to determine K_i, the affinity of the inhibitor for the molecular beacon (K_i = 52 nM).

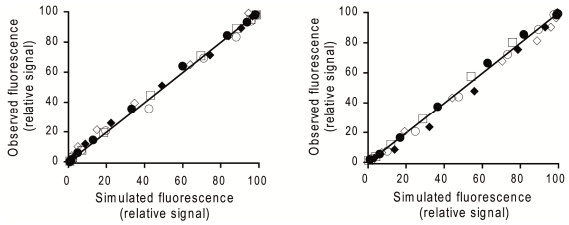

Figure S2. A measure of the "goodness of fit" of the population shift model is provided by the information coefficient, the correlation between our experimentally observed values and those estimated (simulated using the K_d, K_a and K_i values obtained independently) from the model. Shown are the correlations between the observed and estimated values for allosteric inhibition (left) and activation (right) obtained at different concentrations of activator and inhibitor; in all cases the Pearson correlation coefficient is very high ($0.9996>R^2>0.9931$) and there is no statistically significant evidence that any of the fitted slopes differ from unity or any of the fitted intercepts from zero. This suggests that the population shift model readily accounts for the vast majority of the variance across our experimental observations. For clarity, the correlation for only one data set (one inhibitor or activator concentration) has been fitted in each plot. The symbols used for different concentrations of activator and inhibitor are as in Figure 2 and Figure 3.

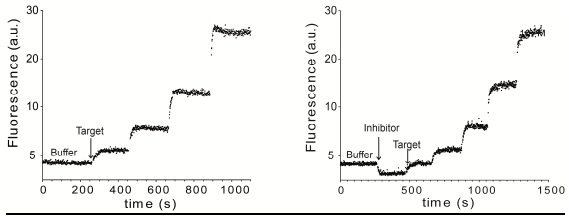

Figure S3. Target, inhibitor and activator binding are all quite rapid. As an example of the reaction times we show here the raw kinetic data obtained with MB#1 (for inhibition studies). (left)) In the absence of inhibitor, the addition of different concentrations of target (to final concentrations of 3, 10, 30, 100 nM) results in a proportional increase in fluorescence that reaches equilibrium in a few minutes. (right) Equilibration after the addition of inhibitor is likewise rapid (here the inhibitor is at 10^{-7} M), as equilibration of the inhibited sensor upon the addition of target (at 10^{-8}, $3x10^{-8}$, 10^{-7}, $3x10^{-7}$, 10^{-6} M).

Allosteric activation: We employed molecular beacon MB#2 for our allosteric activation experiments (see above for sequence). Activator binding in the absence of target produces a small, but easily detectable signal increase in presence of activator (presumably because it moves the fluorophore slightly farther from the quencher). Employing the same procedure described above for the inhibitor, we used this effect to determine the binding curve for the activator and, in turn, defined K_{act} (Figure S4). Binding curves for non-activated sensors and sensors in presence of varying activator concentrations (Figure 3) were obtained using the same procedure described above. More specifically, we used a solution containing 10 nM MB#2 and the relevant concentration of activator and sequentially increased the target concentration via the addition of small volumes of solutions with increasing concentration of target (plus 10 nM MB#2 and the same concentration of activator initially used). Individual binding curves were fitted to Eq. 2 as described above.

Similarly to the considerations described above for the design of our inhibitor, the length of the activator was optimized to ensure that we could precisely measure its affinity for the beacon (K_{act}). Specifically, while lengthening the activator improves its affinity for the molecular beacon, activators longer than the activator described here produced K_{act} below the lowest values we could measure given the 10 nM molecular beacon concentration we employed.

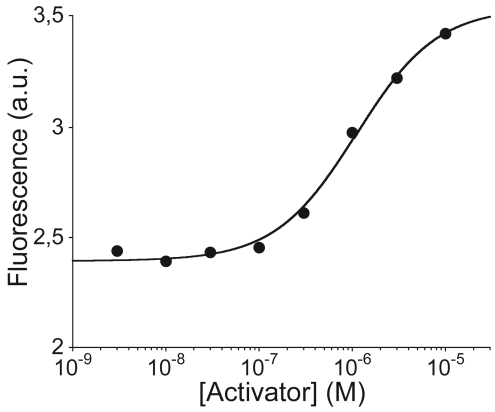

Figure S4. The addition of the allosteric activator causes a small but detectable signal increase (about 3% of the signal change seen for saturating target concentrations). Using this we determined the affinity of the activator for the molecular beacon, K_{act}, to be 1.09 μM.

Inhibition and activation of a single receptor: The molecular beacon used for allosteric inhibition (MB#1, Figure 2) can also be allosterically activated (Figure S5. To do so we employed a 20 bases activator that binds to one of the two, 18-base tails of this beacon and two bases in its stem. This destabilizes the stem and thus pushes the beacon's useful dynamic range to lower target concentrations. Because optimal inhibition requires that we start with a fairly *un*stable stem, and optimal activation requires that we start with a fairly *stable* stem, the range over which this sensor (which was optimized for inhibition) can be activated is smaller than that seen for a sensor that is, instead, optimized for activation (Figure 3).

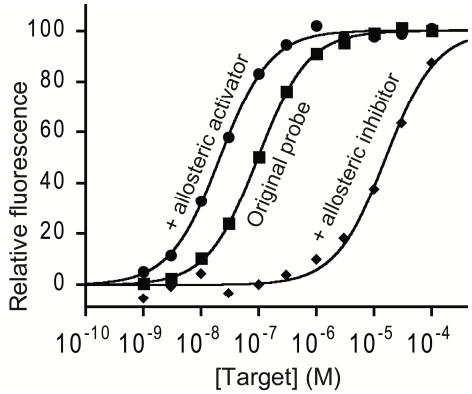

Figure S5. We show here that a single molecular beacon, MB#1, can be both inhibited and activated (using two different single stranded sequences that act as allosteric activator and inhibitor).

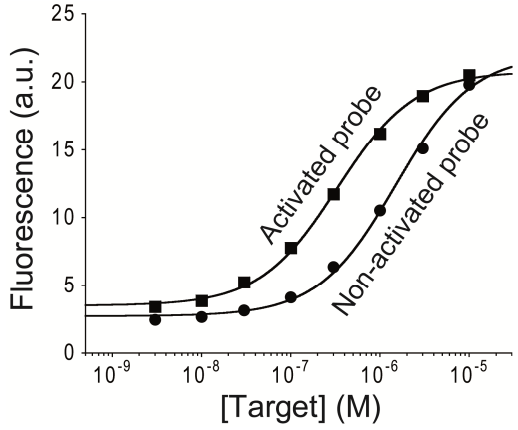

Figure S6. The possibility of dimer formation between the open (target-bound) molecular beacon used for activation experiments (MB #2) is ruled out under the conditions we have employed by the raw fluorescence data. In the presence of activator and saturating target (where the risk of dimerization is greatest) we achieve the same fluorescence signal observed in the presence of saturating amounts of target without activator (conditions under which dimerization would be far less favorable).

Mismatch discrimination: Allosteric mechanisms do not affect molecular beacon specificity. This is demonstrated here by comparing the affinity of our molecular beacon for two DNA targets differing only by one nucleotide (perfect match *versus* one-base mismatch, see above for sequences) (Figure S7).

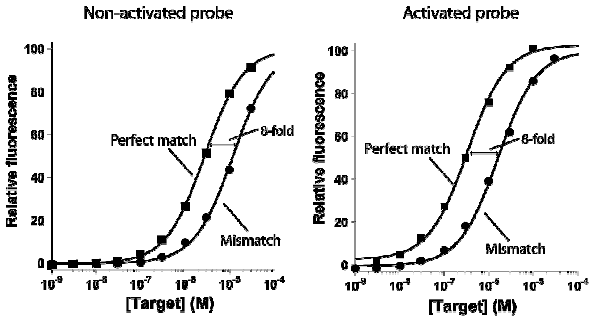

Figure S7. Allosteric control does not alter sensor specificity. The ratio of target dissociation constants obtained for a perfect match and a one-base mismatch target remains fixed at ~8 both in the absence of any allosteric regulator and in the presence of 2.8 μM activator (which produces 75% occupancy of the allosteric site).